Reduced-Order Models of Zero-Net Mass-Flux Jets for Large-Scale Flow Control Simulations

Reni Raju,[1] Ehsan Aram[2] and Rajat Mittal[3]
Department of Mechanical and Aerospace Engineering,
The George Washington University, Washington, DC – 20052

and

Louis Cattafesta,[4]
Interdisciplinary Microsystems Group
Department of Mechanical and Aerospace Engineering,
University of Florida, Gainesville, FL - 32611

Although computational tools are well suited for modeling the dynamics of zero-net mass-flux actuators, the computational costs involved in large-scale flow control simulations necessitate the use of reduced-order models for these devices. A new reduced-order model based on modeling only the slot of ZNMF jets in grazing flows is proposed. A parametric study of dimensionless parameters governing the characteristics of a ZNMF jet in grazing flow was conducted for the reduced-order model along with the commonly used sinusoidal plug flow boundary condition and full cavity simulations. Comparisons of the current model are presented in terms of the vortex dynamics and mean integral quantities, and the performance of the new reduced-order model is encouraging. In addition, the fidelity of the model has also been explored for a canonical separated flow. On the global scale of the flow, the reduced-order model is able to provide a more accurate representation of the full cavity simulation as compared to the conventional boundary condition.

Nomenclature

$C^2(t)$	=	2nd moment of the jet, (m^3/s^2)
$C^3(t)$	=	3rd moment of the jet, (m^4/s^3)
δ	=	Boundary layer thickness, (m)
d	=	Slot width/orifice diameter, (m)
f_J	=	Separation bubble frequency, (Hz)
f_{SL}	=	Shear layer frequency, (Hz)
h	=	Slot/Orifice height, (m)
H	=	Cavity height, (m)
L	=	Length of the prescribed velocity profile, (m)
$\Omega(t)$	=	Instantaneous vorticity flux, (m^2/s^2)
ϕ	=	Phase angle, (°)
p	=	pressure, (N)
Re_δ	=	Boundary layer Reynolds number, $= U_\infty \delta / \upsilon$
Re_J	=	Jet Reynolds number, $= \overline{V_J} d / \upsilon$
S	=	Stokes number, $= \sqrt{2\pi f d^2 / \upsilon}$

[1] Graduate Student, Department of Mechanical & Aerospace Engineering, Student Member AIAA.
[2] Graduate Student, Department of Mechanical & Aerospace Engineering, Student Member AIAA.
[3] Professor, Department of Mechanical & Aerospace Engineering, Associate Fellow AIAA, mittal@gwu.edu
[4] Professor, Department of Mechanical & Aerospace Engineering, Associate Fellow AIAA, cattafes@ufl.edu.

St = Strouhal number, $= 2\pi fd/\overline{V_J}$
u = Streamwise velocity (in x-direction), (m/s)
U_0, V_0 = Velocity amplitudes, (m/s)
U_∞ = Freestream velocity, (m/s)
v = Cross-stream velocity (in y-direction), (m/s)
$\overline{V_J}$ = Spatially and temporally averaged jet velocity, (m/s)
V_{top} = Prescribed velocity amplitude, (m/s)
W = Width of the cavity, (m)
x_c = Center of the prescribed velocity profile, (m)
ξ_z = Spanwise vorticity, (s^{-1})

I. Introduction

ZERO-net mass-flux (ZNMF) actuators or "synthetic jets" have potential applications in the area of mixing enhancement,[1] heat transfer,[2,3] mass transfer,[4] jet vectoring,[5] and active flow control of separation[6-8] and turbulence.[9] The dynamics and performance of these devices depend on several geometrical, structural and flow parameters.[10-12] When compared to the global domain, such as an airfoil, in which the actuator is imbedded, the scales of the actuator are typically $10^{-2} - 10^{-4}$ times smaller in size. Due to the range of scales involved, inclusion of a high-fidelity model of a ZNMF actuator within a macro-scale computational flow model turns out to be an expensive, if not prohibitive, proposition. The desire to compute the flow physics associated with the ZNMF jet control makes reduced-order modeling of these devices a practical necessity in these simulations.

In the past these actuators have been represented as a reduced-order model in simulations in one form or another. Kral *et al.*[13] modeled the actuator via simplified surface boundary conditions for velocity and pressure without the slot and cavity. For variations of the spatial distribution of the velocity profile, it was found that the "top-hat" function provided the closest match to the experiments. Rizzetta *et al.*[14] have used the recorded flow field from a simulation of the isolated jet at the exit of a 2D periodic jet as a boundary condition to an external flow field. On the other hand, Lockerby *et al.*[15] have used a theoretical approach based on classic thin plate theory to model the diaphragm deflection, while the slot is modeled based on unsteady pipe-flow theory. A reduced-order model approximating 2D or 3D synthetic jets via quasi-1D Euler equations was presented by Yamaleev & Carpenter[16]. Filz *et al.*[17] have modeled 2D directed synthetic jets using lumped deterministic source terms (LDST) trained by a neural network. Rathnasingham & Breuer[18] have presented a semi-empirical analytical model of ZNMF actuators using a system of coupled nonlinear state equations describing the structural and fluid characteristics of the device. An analytical lumped element model (LEM) of a piezoelectric-driven synthetic jet has been presented by Gallas *et al.*[10] The model represented the individual components of the synthetic jet as elements of an equivalent electric circuit using conjugate power variables. Sharma[19] has also used an alternate model for LEM. More recently Tang *et al.*[20] have compared the performance of the Dynamic Incompressible Flow model (DI model), Static Compressible Flow Model (SC model) and LEM in predicting the instantaneous space-averaged velocity at the orifice exit. Low-order modeling of two-dimensional synthetic jets via Proper Orthogonal Decomposition (POD) was carried out by Rediniotis *et al.*[21] The dynamical model based on Galerkin projection was derived from the flow for specific Reynolds and Stokes numbers. Kihwan *et al.*[22] have developed a dynamical model based on system identification to identify the interaction of synthetic jets with a laminar boundary layer with potential application to feedback control.

The top-hat profile used by Kral *et al.*[13] is the simplest model of the jet and is referred to as the "zeroth-order model" in the current study. Such a representation eliminates the need of simulating the cavity and the slot. A similar approach has also been adopted in some previous studies.[23,24] However, it is not clear to what extent such a boundary condition accurately models the key features of the jet. Since the control mechanism of the actuator depends on transfer of the momentum or vorticity flux to the external boundary layer, it is essential that any such model should be able to represent these quantities accurately.

The purpose of the current study is to explore the issues of actuator modeling via numerical simulations. Based on these simulations we propose a new model for ZNMF jets in grazing flows. The model is compared with the ful cavity simulations and the zeroth-order model in attached flows. In addition, the effectiveness of the proposed model with the modified boundary condition representation versus full cavity simulations has also been studied for a separated boundary layer in a canonical flow configuration.

II. Slot-Only ZNMF Actuator Model

The major reason for the shortcoming of the modified boundary condition models is the neglect of the flow physics associated with the slot. Our previous studies[25] show that flow in the slot tends to separate at the top and bottom lips, and the formation of secondary vortices near the exit tends to significantly alter the flow field. Thus the working hypothesis for the current reduced-order model is that the inclusion of just the slot with appropriate boundary conditions should significantly improve the fidelity of the actuator model. This hypothesis is supported by past studies[26,27] that have shown that the shape of the cavity has very little effect on the flow emanating from the jet provided that the incompressible flow assumption inside the actuator cavity is valid. The approach used for the current study explores the significance of the slot via simplified boundary conditions and hence effectively reduces the computational complexity. An attempt is thus made to replicate the flow physics inside the slot to further improve the fidelity of the model.

Consider the flow inside the 2D slot of a typical ZNMF actuator as seen in Figure 1(a). The area change from the cavity to the slot causes the flow to turn near the bottom lip of the slot, and the flow pattern during expulsion is similar to the one caused by a sink present somewhere along the slot center during the expulsion phase. Hence the flow enters the slot radially at any given time during expulsion and, in terms of its Cartesian components, will have two components of velocity, u and v. As seen in Figure 1(a), at the entrance to the slot the u -velocity will be significant, while near the slot center the v -velocity will dominate. Thus an approximation of this flow pattern prescribes a corresponding boundary condition profile for the u - velocity which varies linearly in the x-direction from a maximum positive value near the left wall to a minimum negative value near the right wall (see Table 1).

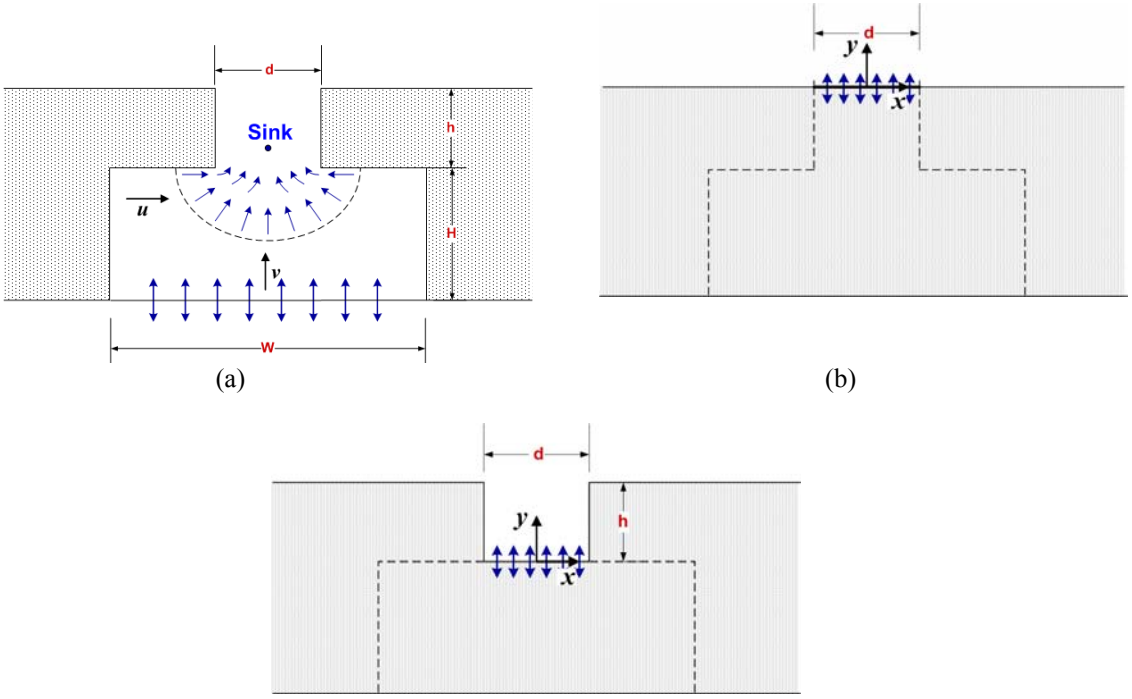

Figure 1: Schematic showing (a) the typical flow pattern seen in a ZNMF jet slot for a full cavity (FC) configuration and (b) modified boundary condition (MBC) and (c) Proposed slot-only (SO) model.

A. Model Comparison

Based on the above arguments, three separate flow configurations have been chosen for comparison. These include the full-cavity (FC), the slot-only (SO) and modified boundary condition (MBC) configurations. As the name suggests, the FC model consists of full-cavity simulations and is a complete representation of a 2D ZNMF jet, as seen in Figure 1(a). The driver displacement is represented as an oscillatory boundary condition at the bottom of the cavity and has been found to be a fairly accurate representation when compared with experimental results.[26] On

the other hand Figure 1(b) shows the MBC configuration, which consists of prescribing only the vertical component of the velocity over the exit plane of the jet, as mentioned earlier. The proposed SO model is based on the configuration shown in Figure 1(c). For this configuration the slot is modeled by considering the full length of the slot, i.e., h/d =100%, which is necessary for the replicating the sink type behavior of a FC configuration. Two variants of the slot-only models are considered. For the first, called the SO-1 model, only the sinusoidal *v*-velocity is prescribed at the bottom while for the second, the SO-2 model, boundary conditions for both the *u*- & *v*-velocities during expulsion have been used. Here the *u*-velocity is prescribed as a linearly varying sinusoidal profile that satisfies no-slip condition at the boundary. Table 1 lists the boundary conditions used for the different configurations during both expulsion and ingestion phases with the corresponding location.

Table 1: Boundary conditions used for the different configurations considered for current work.

Model	y/d location w.r.t to FC	Expulsion		Ingestion	
		$v(x,t)$	$u(x,t)$	$v(x,t)$	$\frac{\partial u}{\partial y}(x,t)$
FC	0	$V_0\sin(\omega t)$	0	$V_0\sin(\omega t)$	-
MBC	$h+H$	$V_0\sin(\omega t)$	0	$V_0\sin(\omega t)$	0
SO-1	H	$V_0\sin(\omega t)$	0	$V_0\sin(\omega t)$	0
SO-2	H	$V_0\sin(\omega t)$	$\frac{-x}{d/2}U_0\sin(\omega t)$, for $-\frac{d}{2}<x<\frac{d}{2}$ 0, at $x=\frac{d}{2}\,\&\,-\frac{d}{2}$	$V_0\sin(\omega t)$	0

Care has been taken to ensure that the mass flow rate at the exit of the slot for the FC configuration and reduced-order models are the same. The dimensionless parameters of significance for a ZNMF jet under quiescent condition are the Strouhal number, St, jet Reynolds number, Re_J, velocity ratio, $U_\infty/\overline{V_J}$ and boundary-layer thickness to jet width ratio, δ/d. Table 2 lists the cases along with the corresponding parameters used for the current study. It is known that the jet characteristics are determined by functional dependence on the parameters as $fn\left(\mathrm{St},\frac{U_\infty}{\bar{V}_j},\frac{\delta}{d},\mathrm{Re}_j\right)$.[25] Hence for the current study three different simulation sets were considered for each of these parameters while keeping the rest constant. The velocity amplitude ratio $U_0/V_0=1$ was maintained for all the cases.

Table 2: Parameters used for reduced-order modeling simulations

Case	Re_J	S	$U_\infty/\overline{V_J}$	δ/d	Re_δ	St
1	125	10	4	2	1000	0.8
2	281.25	15	4	2	2250	0.8
3	**500**	**20**	**4**	**2**	**4000**	**0.8**
4	125	20	4	2	1000	3.2
5	250	20	4	2	1500	1.6
6	500	20	2	2	4000	0.8
7	500	20	3	2	4000	0.8
8	500	20	4	1	4000	0.8
9	500	20	4	3	4000	0.8

All the computations use a single grid of dimensions 178 × 178 for the FC simulations and a domain size of $9d \times 10d$. For the remaining configurations the grid resolution in the slot and external flow field is held constant at all times. The direct numerical simulations are used to model synthetic jets issuing from a cavity. Incompressible Navier-Stokes equations are solved in time using a second-order accurate fractional step method. In a Cartesian framework, a second-order Adams-Bashforth scheme is employed for the convective terms, while the diffusion terms are discretized using an implicit Crank-Nicolson scheme that eliminates the viscous stability constraint. The solver has been rigorously validated by comparisons of several test cases against established experimental and computational data including synthetic jets.[26,28]

B. Canonical Separated Flow Configuration

Whereas the above study examines the performance of the different modes for an attached grazing flow, a relevant issue to be examined is to what extent the details of the actuator model modify the effect of the jet on a separation bubble. In order to address this issue we have also examined a case where a separation bubble is created downstream of the jet by prescribing a blowing-suction boundary condition on the top boundary of the domain. A zero-vorticity condition, along the lines of Na & Moin[29] is applied on this boundary as follows:

$$v(x, L_y) = G(x), \qquad \left.\frac{\partial u}{\partial y}\right|_{(x, L_y)} = \frac{dG}{dx} \tag{1}$$

where $G(x)$ is the prescribed blowing and suction velocity profile defined in the form of:

$$G(x) = -V_{top} \sin\left(\frac{2\pi(x - x_c)}{L}\right) e^{-\alpha\left\{\frac{2(x-x_c)}{L}\right\}^{\beta}} \tag{2}$$

where L is the length and x_c is the center of the velocity profile. The parameters V_{top}, α and β are set to U_∞, 10 and 20, respectively. Figure 2 shows the configuration used to generate the separated flow. The FC, SO-2 and MBC model configurations were tested under these conditions. The simulations have been carried out on the domain with $100d \times 32d$ size using a grid of dimensions 321 × 257 for FC case and same resolution for two other configurations.

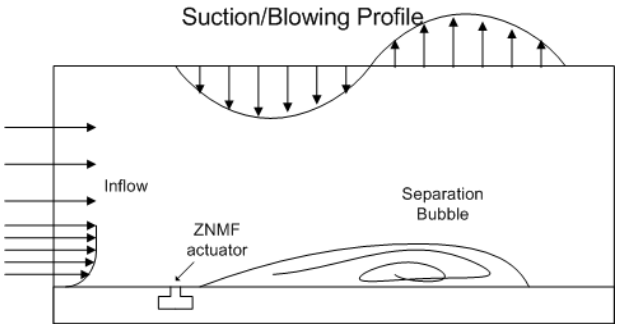

Figure 2: Flow configuration used for simulating a canonical separated flow.

III. Results

A. Model Performance in Attached Grazing Flow

Holman et al.[12] have shown that the jet formation criterion is determined by the relation, $\mathrm{Re}_J / S^2 = 1/St > K$ and is proportional to the non-dimensional vorticity flux. Here, K is a constant found to be $O(1)$ for 2D jets and ~0.16 for axisymmetric jets. Thus for the given set of conditions of St =0.8, a jet is formed and is able to impart a significant amount of vorticity flux to external flow. Figure 3 shows the comparison of the spanwise vorticity at the peak expulsion (ϕ =90°) and peak ingestion (ϕ =270°) for all models at Re_J =500, S =20, $U_\infty / \overline{V_J}$ =4.0 and δ/d =2.0. The flow tends to separate near the bottom lip of the slot for the full cavity simulations. The separating shear layers tend to roll up on either wall during expulsion at the exit plane of the slot and a strong clockwise vortex

is formed that is swept away by the incoming boundary layer. The MBC model, seen in Figure 3(b), forms a smaller clockwise vortex near the lip of the slot in comparison to the FC model. The SO models are able to reproduce the flow physics of the baseline flow in the proximity of the slot exit, as seen in Figure 3(c) & (d). Unlike the FC model, inside the slot the boundary layer remains attached to the walls for SO-1 model. On the other hand the SO-2 does show flow separation on the slot walls but is unable to capture roll up of the boundary layer on the walls. This difference can be attributed to larger incoming angle of the flow from the cavity for the FC model. The ingestion phase for the SO models shows a near perfect match with the FC model within the slot, proving the validity of using a simple Neumann boundary condition for the *u*-velocity. The SO models are able to capture even the secondary vortex produced during expulsion, although for the SO-2 model the vortex loses its strength downstream.

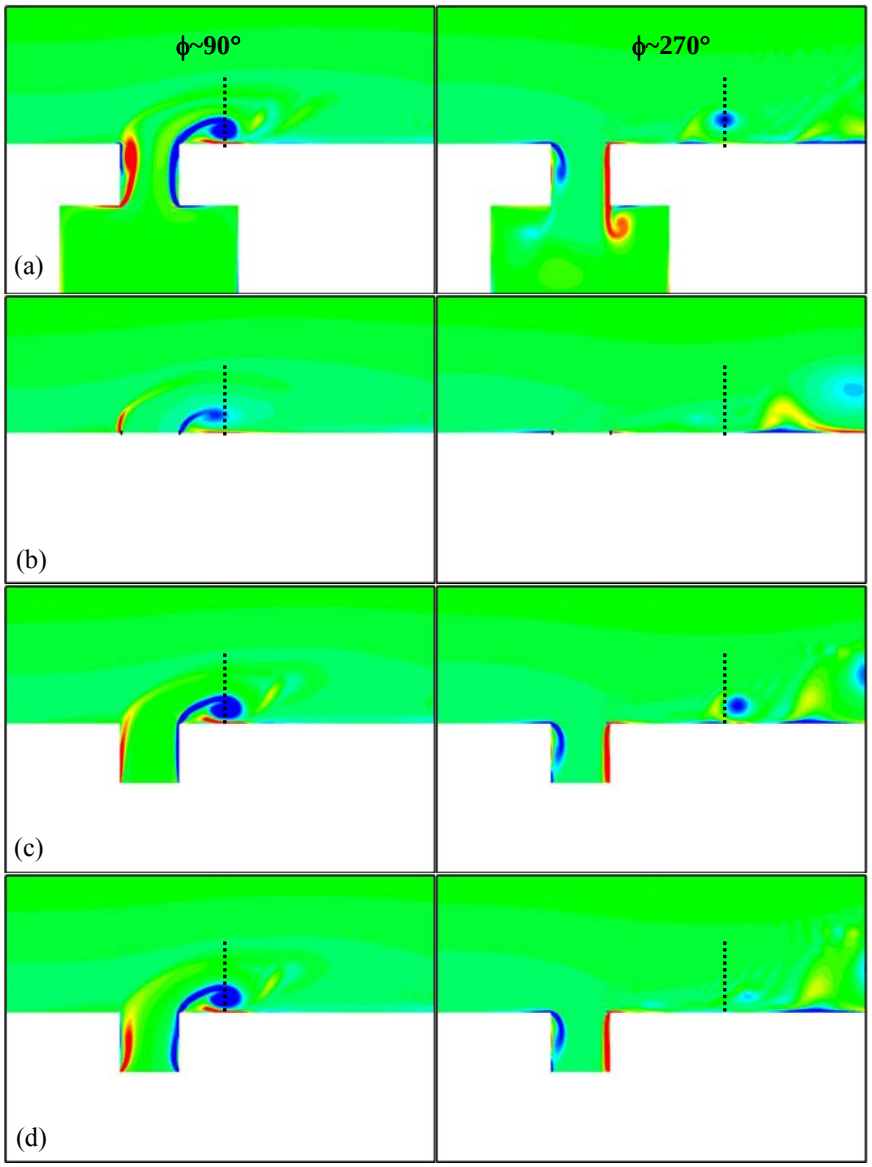

Figure 3: Instantaneous spanwise vorticity during peak expulsion and peak ingestion for (a) FC, (b) MBC model (c) SO-1 model and (d) SO-2 model for Re_J =500, S =20, $U_\infty/\overline{V_J}$ =4.0 and δ/d =2.0. Dashed lines compare the locations of vortex structures for the three models with respect to FC configuration.

The characteristics of the jet can be therefore defined on the basis of the integral quantities such as vorticity flux, momentum flux and kinetic energy flux. The unsteady variations of these quantities are compared for the representative cases in Figure 4. Note the definitions for momentum flux and kinetic energy flux are $\rho C^2(t) = \rho \int_{-d/2}^{d/2} [v(x,t)]^2 dx$ and $\rho C^3(t) = \rho \int_{-d/2}^{d/2} [v(x,t)]^3 dx$ and have been normalized by a suitable quantity. On the other hand the vorticity flux is defined as $\Omega(t) = \int_{-d/2}^{d/2} \xi_z(x,t) v(x,t) dx$. Figure 4 shows that the accumulation of vorticity from shear layer separation causes peaks in the integral quantities for the FC model during expulsion. Similar features are seen for the SO-2 model and, although they are lower in magnitude, they appear to give a closer match to the FC model than the SO-1 model during expulsion. On the other hand the MBC model is unable to predict the flow behavior in the slot during most of the cycle. Hence although the flow field is significantly altered by secondary vortices, the integral measures can be reasonably approximated by using the SO-2 model; although for a better match the incoming flow angle, i.e. U_0/V_0 ratio, might need to be modified further.

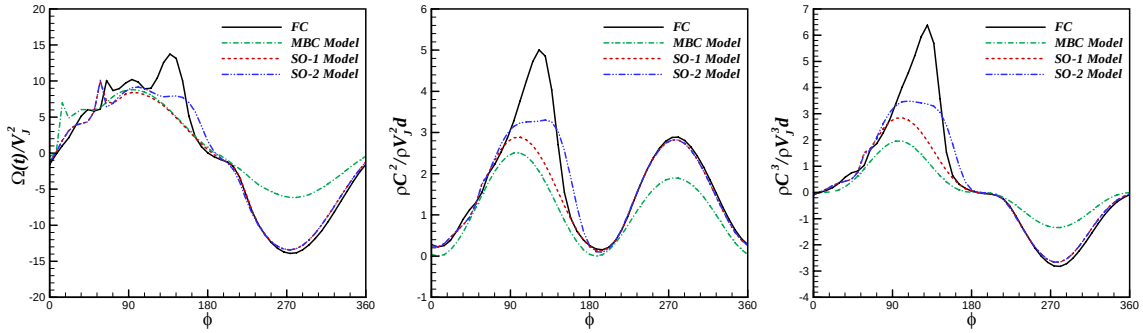

Figure 4: Comparison of the vorticity flux (left), momentum flux (middle) and kinetic energy flux (right) for all models as a function of phase for $\mathbf{Re}_J$ =500, S =20, $U_\infty/\overline{V_J}$ =4.0, δ/d =2.0, St =0.8.

Simulations at higher Strouhal number (St =3.2) are presented in Figure 5 where Re_J =125, S =20, $U_\infty/\overline{V_J}$ =4.0 and δ/d =2.0. This corresponds to the no-jet formation case due to the high St, and during peak expulsion the boundary layers near the bottom lips thicken to form a vena-contracta. At the exit, the shear layer rolls up to form a relatively small clockwise vortex which does not travel far from the slot during the suction stroke. Note that the expulsion stroke is defined as $0^\circ \le \phi < 180^\circ$ and suction stroke as $180^\circ \le \phi < 360^\circ$. Interestingly it is found that all the models give a reasonable approximation to the FC model at the slot exit during the expulsion phase of the cycle. However, the MBC model does not produce coherent vortex structures as seen for the rest of the configurations near the right exit lip which is apparent during the suction stroke, as seen in Figure 5(b). The SO-2 model captures the vena-contracta of the flow near the slot inlet which, although not seen for the SO-1 model, does not seem to significantly affect the external flowfield. Both models replicate the flow behavior of FC model during the suction stroke.

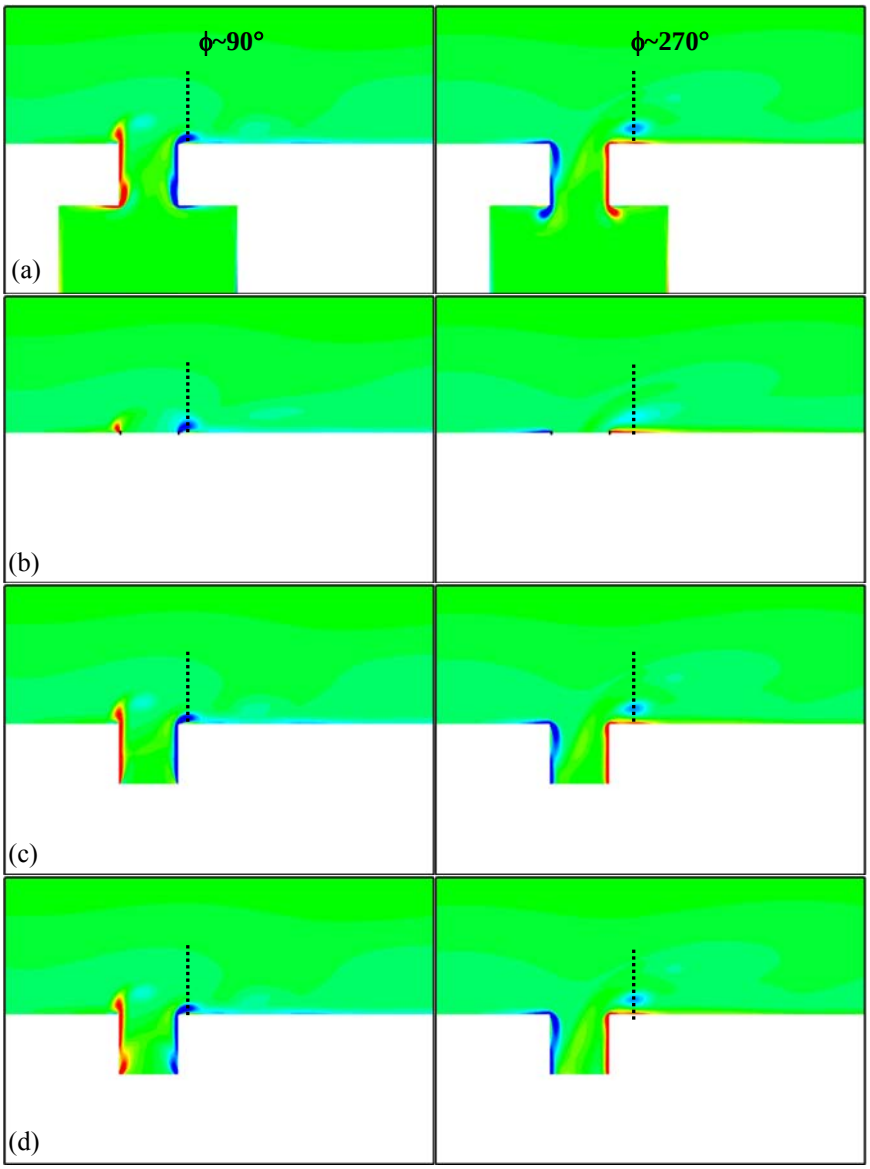

Figure 5: Instantaneous spanwise vorticity during peak expulsion and peak ingestion for (a) FC, (b) MBC model (c) SO-1 model and (d) SO-2 model at $\mathbf{Re}_J$ =125, S =20, $U_\infty/\overline{V_J}$ =4.0, δ/d =2.0. Dashed lines compare the locations of vortex structures for the three models with respect to FC configuration.

At higher Strouhal numbers, as is the case for Re_J =125, S =20, $U_\infty/\overline{V_J}$ =4.0 and δ/d =2.0, seen in Figure 6, the integral measures do not show peaks during the expulsion cycle. An increase in St tends to decrease the contribution of vorticity flux of the jet to the external boundary layer. This also remains true for the momentum and kinetic energy fluxes. Both the SO models compare reasonably well with the FC model during the whole cycle. On the other hand, the MBC model shows a slight phase shift during the expulsion phase for the vorticity flux, while it produces slightly larger deviations for the momentum and kinetic energy fluxes.

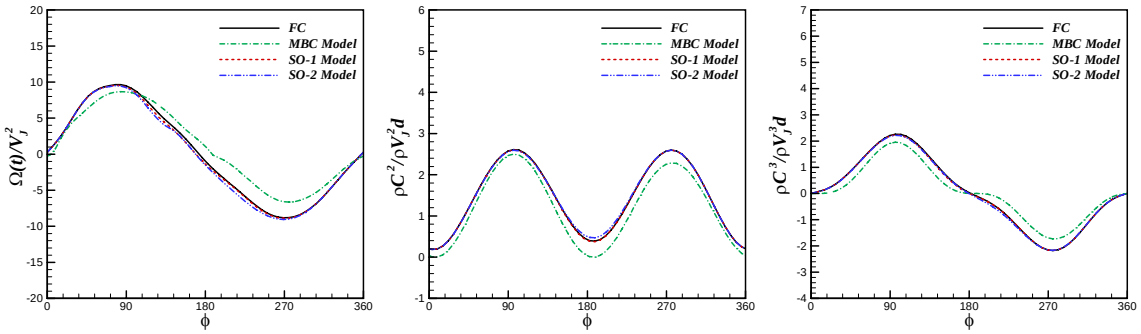

Figure 6: Comparison of the vorticity flux (left), momentum flux (middle) and kinetic energy flux (right) for all models as a function of phase for $\mathbf{Re}_J$ =125, S =20, $U_\infty/\overline{V_J}$ =4.0, δ/d =2.0, St =3.2.

Similar analyses have been conducted for the other cases. Figure 7(a) and (b) compare the integral quantities for Re_J =125, S =10, $U_\infty/\overline{V_J}$ =4.0, δ/d =2.0 and Re_J =281.5, S =15, $U_\infty/\overline{V_J}$ =4.0, δ/d =2.0, respectively, where St =0.8 for both the cases. When compared with Re_J =500, S =20, $U_\infty/\overline{V_J}$ =4.0, δ/d =2.0 shown in Figure 4, it can be seen that, although the Strouhal number remains the same, as Re_J increases the vorticity flux during the expulsion phase also tends to increase and distort the sinusoidal profile. These peaks correspond to the expulsion of vortices from the exit plane of the jet. On the other hand the suction phase behavior remains the same for these cases. In terms of model performance for Re_J =125, S =10, $U_\infty/\overline{V_J}$ =4.0 and δ/d =2.0 the SO-2 model tends to slightly overpredict the integral measures versus the FC model during the expulsion phase, while the SO-1 model slightly underpredicts these values. Surprisingly the MBC model also shows a reasonable match for the vorticity flux during the expulsion phase but not for the other quantities. During ingestion the SO models match the FC quantities at all times. However, this is not the case for the MBC model. For Re_J =281.5, S =15, $U_\infty/\overline{V_J}$ =4.0 and δ/d =2.0, similar behavior is observed with the SO-2 model providing the best approximation. At higher Strouhal numbers, as is the case for Re_J =250, S =20, $U_\infty/\overline{V_J}$ =4.0 and δ/d =2.0, seen in Figure 7(c) where St =1.6, the integral measures show slightly lower values. Note that for this case the vorticity flux again shows several peaks during the expulsion phase indicating that the jet is formed under these conditions. The integral quantities of both SO models compare reasonably well with the FC model during the whole cycle and are able to capture the small peaks in the vorticity flux. Note that for this case, the behavior of both model is similar, indicating that under these conditions the shear layer separation at the bottom lip is not as important as the cases with St =0.8 where the SO-1 model does not perform as well as the SO-2 model. This is apparent from Figure 6 where both these models show similar representation of the flow physics.

In addition to the significance of Re_J and St, the effects of freestream to jet velocity ratio, $U_\infty/\overline{V_J}$ and the boundary layer thickness to jet diameter ratio, δ/d are presented in Figure 8. The variation in the velocity ratio is presented in the Figure 8(a) and (b) for Re_J =500, S =20, $U_\infty/\overline{V_J}$ =2.0, δ/d =2.0 and Re_J =500, S =20, $U_\infty/\overline{V_J}$ =3.0, δ/d =2.0 respectively. Due to the lower freestream velocity, the magnitudes of the peaks are reduced. It can be observed that increasing the velocity ratio leads to an increase in the momentum and kinetic energy fluxes. For these cases the SO-2 model is able to yield a better approximation to the FC configuration, while both the SO-1 and MBC models significantly underpredict the moments during the expulsion phase.

On the other hand, decreasing the boundary layer thickness significantly alters the integral quantities and leads to an increase in the integral measures over a cycle with sharper peaks as seen in Figure 8(c) and (d) for two different ratios δ/d =1.0 and δ/d =3.0, respectively. The predictive capabilities of the models deteriorate as the boundary layer thickness is reduced, although the SO-2 model consistently gives better performance over other models. Overall the ingestion phase of both SO models compares well with the FC model. This implies that the inclusion of the slot is a significant factor for improvement of the model, while accounting for the separation at the bottom lip of the slot increases the fidelity of the model still further.

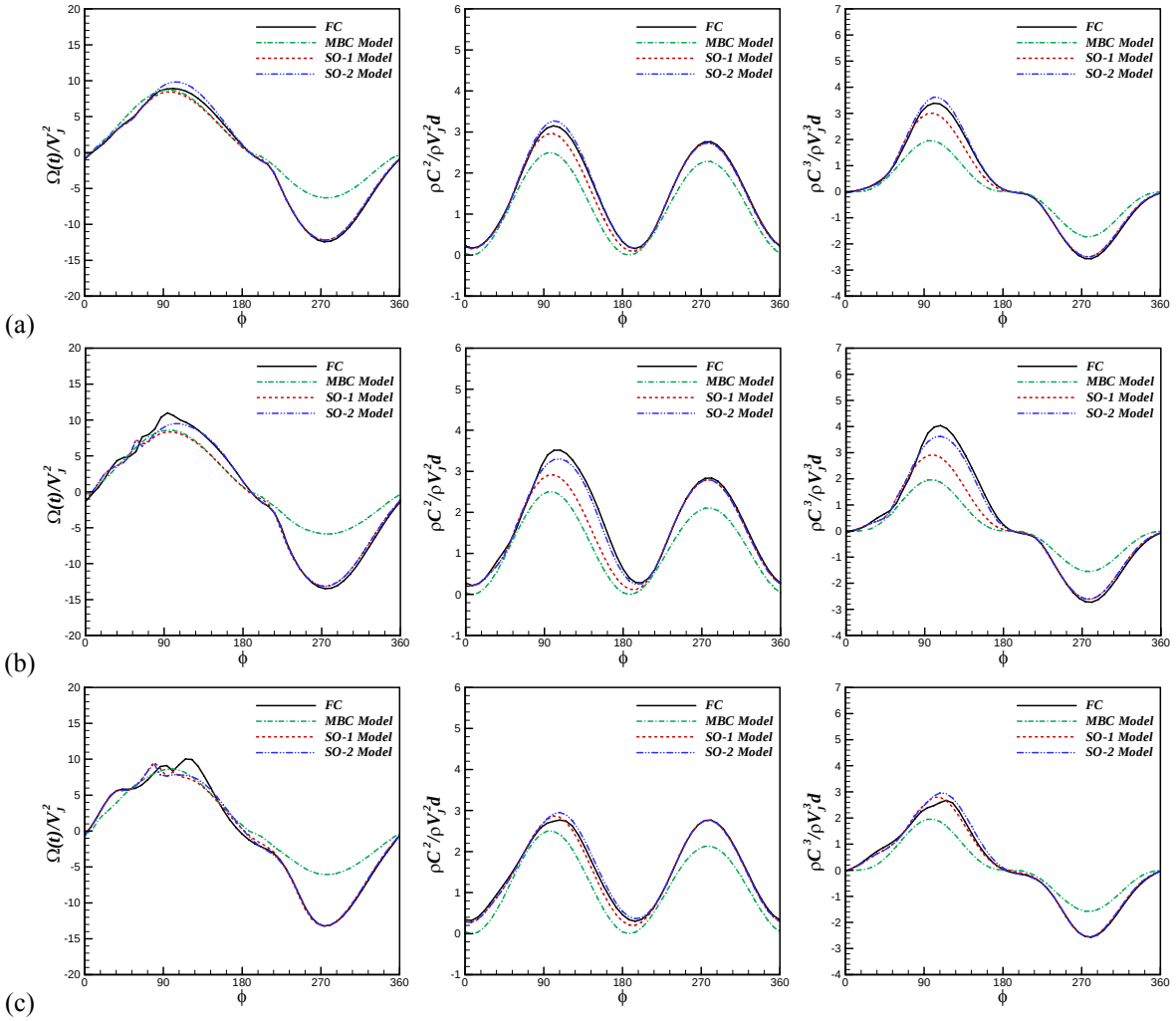

Figure 7: Comparison of the vorticity flux (left), momentum flux (middle) and kinetic energy flux (right) for all models as function of phase for (a) Re_J =125, S =10, $U_\infty/\overline{V_J}$ =4.0, δ/d =2.0, St =0.8, (b) Re_J =281.25, S =15, $U_\infty/\overline{V_J}$ =4.0, δ/d =2.0, St =0.8, and (c) Re_J =250, S =20, $U_\infty/\overline{V_J}$ =4.0, δ/d =2.0, St =1.6.

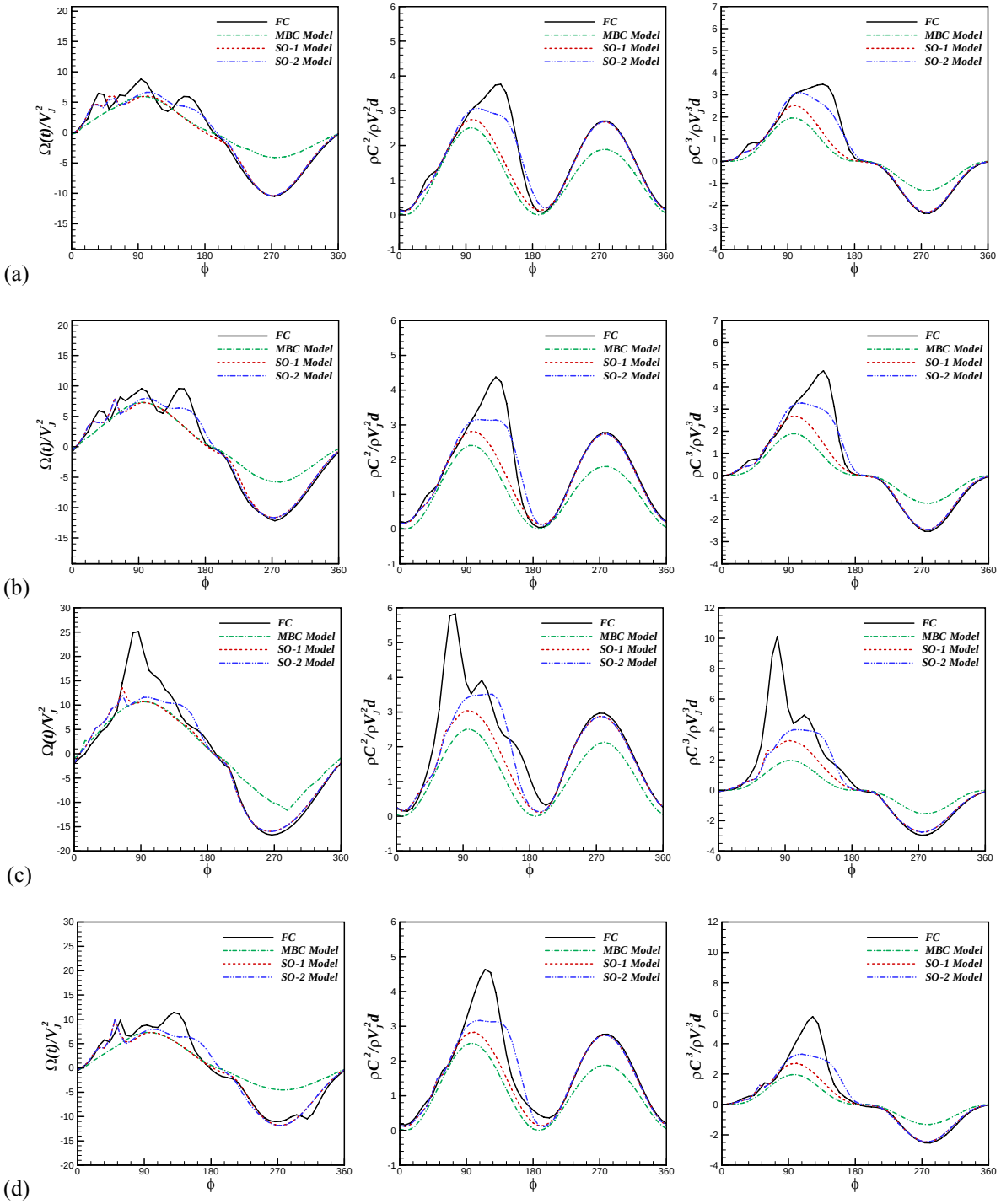

Figure 8: Comparison of the vorticity flux (left), momentum flux (middle) and kinetic energy flux (right) for all models as function of phase for (a) Re_J =500, S =20, $U_\infty/\overline{V_J}$ =2.0, δ/d =2.0, St =0.8, (b) Re_J =500 S =20, $U_\infty/\overline{V_J}$ =3.0, δ/d =2.0, St =0.8, (c) Re_J =500, S =20, $U_\infty/\overline{V_J}$ =4.0, δ/d =1.0, St =0.8 and (d) Re_J =500, S =20, $U_\infty/\overline{V_J}$ =4.0, δ/d =3.0, St =0.8.

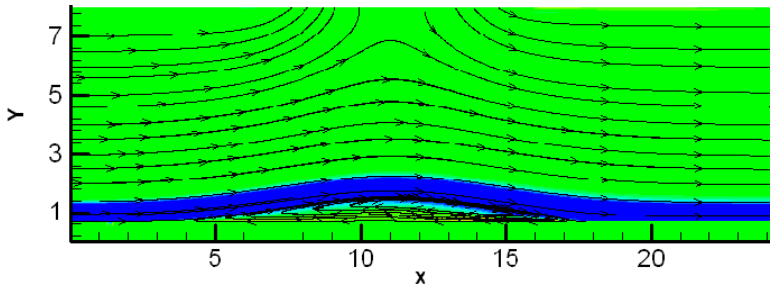

Figure 9: Spanwise vorticity and mean streamlines for the unforced separated flow.

B. Model Performance for a Canonical Separated Flow

As seen in Figure 9, a separation bubble was created by imposing the boundary condition described in Eq. (1)-(2) with length, $L_{sep} = 54d$. The effect of forcing of the ZNMF jet, placed approximately $2.5d$ upstream of the point of separation, on the separation bubble has been examined for different model configurations. As seen in the previous section, since the SO-2 model performs superior to other models, it was tested along with FC and MBC configurations for six different forcing frequencies based on shear layer frequency, such that $f_J = \varepsilon f_{SL}$. The six values of ε were chosen as 0.25, 0.5, 0.75, 1, 1.25 and 1.5. For all the cases examined for the separated flow, the rest of the flow characteristics were held fixed at $\mathrm{Re}_J = 125$, $U_\infty / V_J = 4$ and $\delta / d = 3$. Figure 10 shows contours of instantaneous spanwise vorticity at peak expulsion and mean streamlines for these three cases at one particular forcing frequency ($f_J = 0.25 f_{SL}$). By comparing the mean streamlines it can be seen that FC and SO-2 configuration yield a very similar effect on the separation bubble. For both these cases the size of the separation bubble is reduced by a factor of 2.6. On the other hand the MBC model, as expected, is unable to match the FC model, where the separation bubble size is reduced by a factor of 2. It is clear that the SO-2 model is able to able to provide a better representation of the ZNMF actuator on a global scale.

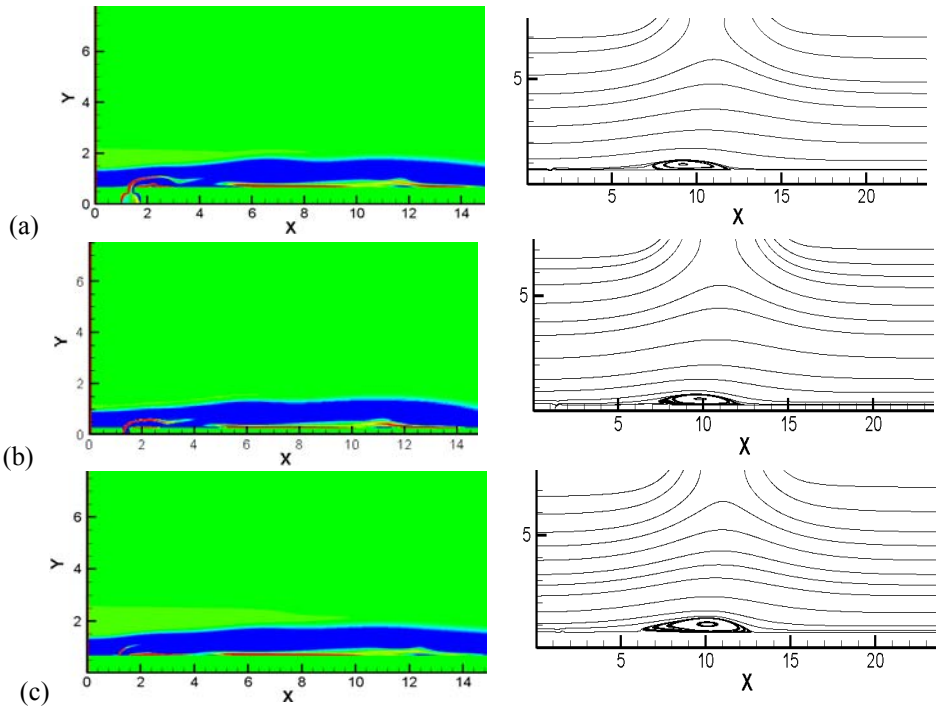

Figure 10: Instantaneous spanwise vorticity and mean streamlines for the a) FC, b) SO-2, and c) MBC models for $f_J = 0.25 f_{SL}$.

Figure 11 compares the performance of three models for different forcing frequencies. The separation bubble frequency in this figure is defined, based on the separation bubble size, as $f_{sep} = U_\infty / L_{sep}$. It is found that the SO-2 model gives a good approximation to the FC model for separation bubble control at all forcing frequencies, especially for $\varepsilon \leq 0.5$. The maximum percentage difference of separation bubble size seen between SO-2 and FC model is approximately 8%. On the other hand the MBC model underestimates the performance of FC on separation control for low frequencies ($f_J < f_{SL}$) where control is most effective. Overall the percentage difference of separation bubble size for the MBC model varies from 3 – 43%. It is also clear that the separation bubble size is reduced by decreasing the jet frequency, and maximum reduction in this particular problem and this frequency range is approximately 60%.

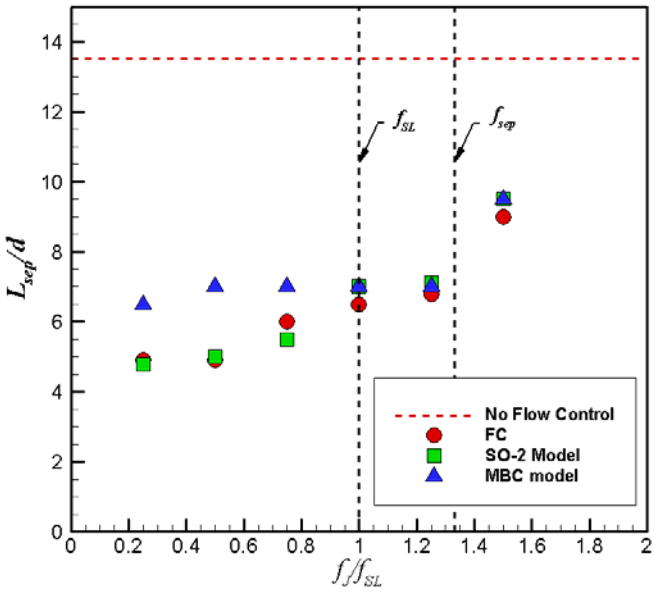

Figure 11: Effect of forcing frequency on the separation bubble size for three models.

IV. Conclusions

A simple reduced-order model is presented for the representation of ZNMF jets in large-scale flow control simulations. The model includes the slot of the actuator due to its importance in governing the dynamics of the interaction process with a grazing flow. Two variants of the slot-only model were considered, and a parametric numerical study was carried out to determine the performance of each model compared to a conventional modified boundary condition. It was found that, unlike the conventional MBC model, the slot-only models were able to capture more of the flow physics associated with full cavity simulations. A comparison of the integral measures of vorticity, momentum, and kinetic energy fluxes for these models showed that the slot-only model that assumes a sink-like flow at the slot inlet (i.e., the SO-2 model) provides the best modeling approximation. The performance of the model was also compared with full cavity simulations and the simple MBC model for a canonical separated flow at different forcing frequencies. It was found that at lower forcing frequencies, the flow separation extent was reduced significantly, and the SO-2 model was able to predict the separation bubble size reduction with improved accuracy. Future work in this direction will focus on determining the appropriate value of U_0/V_0, used in SO-2, as a function of the dimensionless flow parameters to study the effect of incoming flow angle at the bottom lip of the slot.

Acknowledgments

This work is supported by grants from AFOSR and a NASA Cooperative Agreement NNX07AD94A monitored by Dr. Brian Allan.

References

[1]Chen, Y., Liang, S., Aung, K. , Glezer, A. , and Jagoda, J, "Enhanced Mixing in a Simulated Combustor Using Synthetic Jet Actuators." AIAA Paper 99-0449, 1999.

[2]Campbell, J.S., Black, W.Z., Glezer, A., and Hartley, J.G., "Thermal Management of a Laptop Computer with Synthetic Air Microjets." *Intersociety Conference on Therm. Phenomenon, IEEE*, 1998, pp. 43-50.

[3]Mahalingam, R., and Glezer, A., "Design and Thermal Characteristics of a Synthetic Jet Ejector Heat Sink." *Journal of Electronic Packaging*, Vol. 127, No. 2, 2005, pp. 172-177.

[4]Trávníček, Z., and Tesař, V., "Annular Synthetic Jet Used for Impinging Flow Mass–Transfer." *International Journal of Heat and Mass Transfer*, Vol. 46, No. 17, 2003, pp. 3291-3297.

[5]Smith, B.L., and Glezer, A., "Jet Vectoring Using Synthetic Jets." *Journal of Fluid Mechanics*, Vol. 458, 2002, pp. 1-24.

[6]Seifert, A., Bachar, T., Koss, D., Shepshelovich, M., and Wygnanski, I., "Oscillatory Blowing: A Tool to Delay Boundary-Layer Separation." *AIAA Journal*, Vol. 31, No. 11, 1993, pp. 2052-2060.

[7]Seifert, A., Darabi, A., and Wygnanski, I., "Delay of Airfoil Stall by Periodic Excitation." *Journal of Aircraft*, Vol. 33, No. 4, 1996, pp. 691-698.

[8]Honohan, A.M., Amitay, M., and Glezer, A., "Aerodynamic Control Using Synthetic Jets." AIAA Paper 2000-2401, 2000.

[9]Rathnasingham, R., and Breuer, K.S., "System Identification and Control of a Turbulent Boundary Layer." *Physics of Fluids*, Vol. 9, No. 7, 1997, pp. 1867-1869.

[10]Gallas, Q., Holman, R., Nishida, T., Carroll, B., Sheplak, M., and Cattafesta, L., "Lumped Element Modeling of Piezoelectric-Driven Synthetic Jet Actuators." *AIAA Journal*, Vol. 41, No. 2, 2003, pp. 240-247.

[11]Glezer, A., and Amitay, M., "Synthetic Jets." *Annual Review of Fluid Mechanics*, Vol. 34, 2002, pp. 503-529.

[12]Holman, R., Utturkar, Y., Mittal, R., Smith, B.L., and Cattafesta, L., "Formation Criterion for Synthetic Jets." *AIAA Journal*, Vol. 43, No. 10, 2005, pp. 2110-2116.

[13]Kral, L.D., Donovan, J.F., Cain, A.B., and Cary, A.W., "Numerical Simulation of Synthetic Jet Actuators." AIAA Paper 97-1824, 1997.

[14]Rizzetta, D.P., Visbal, M.R., and Stanek, M.J., "Numerical Investigation of Synthetic-Jet Flow Fields." *AIAA Journal*, Vol. 37, No. 8, 1999, pp. 919-927.

[15]Lockerby, D. A., Carpenter, P.W., and Davies, C., "Numerical Simulation of the Interaction of Microactuators and Boundary Layers." *AIAA Journal*, Vol. 40, No. 1, 2002, pp. 67-73.

[16]Yamaleev, N.K., and Carpenter, M.H., "A Reduced-Order Model for Efficient Simulation of Synthetic Jet Actuators." *NASA Technical Reports, NASA/TM-2003-212664*, 2003.

[17]Filz, C., Lee, D., Orkwis, P.D., and Turner, M.G., "Modeling of Two Dimensional Directed Synthetic Jets Using Neural Network-Based Detereministic Source Terms." AIAA Paper 2003-3456, 2003.

[18]Rathnasingham, R., and Breuer, K.S., "Coupled Fluid-Structural Characteristics of Actuators for Flow Control." *AIAA Journal*, Vol. 35, No. 5, 1997, pp. 832-837.

[19]Sharma, R. N. , "Fluid-Dynamics-Based Analytical Model for Synthetic Jet Actuation." *AIAA Journal*, Vol. 45, No. 8, 2007, pp. 1841-1847.

[20]Tang, H., Zhong, S., Jabbal, M., Garcillan, L., Guo, F., Wood, N. J., and Warsop, C. , "Towards the Design of Synthetic-Jet Actuators for Full-Scale Flight Conditions. Part 2: Low-Dimensional Atuator Prediction Models and Actuator Design Methods." *Flow, Turbulence and Combustion*, Vol. 78, No. 3, 2007, pp. 309-329.

[21]Rediniotis, O.K., Ko, J., and Kurdila, A.J., "Reduced Order Nonlinear Navier-Stokes Models for Synthetic Jets." *Journal of Fluids Engineering*, Vol. 124, No. 2, 2002, pp. 433-443.

[22]Kihwan, K., Beskok, A., and Jayasuriya, S., "Nonlinear System Identification for the Interaction of Synthetic Jets with a Boundary Layer." American Control Conference, 2005. Proceedings of the 2005, 2005.

[23]Rampunggoon, P., "Interaction of a Synthetic Jet with a Flat-Plate Boundary Layer." Phd Thesis, Department of Mechanical Engineering, University of Florida, 2001.

[24]Ravi, B.R., "Numerical Study of Three Dimensional Synthetic Jets in Quiescent and External Grazing Flows." DSc Thesis, Mechanical and Aerospace Engineering, The George Washington University, 2007.

[25]Raju, R., Mittal, R., Gallas, Q., and Cattafesta, L., "Scaling of Vorticity Flux and Entrance Length Effects in Zero-Net Mass-Flux Devices." AIAA Paper 2005-4751, 2005.

[26]Kotapati, R.B., Mittal, R. , and Cattafesta, L., "Numerical Study of Transitional Synthetic Jet in Quiescent External Flow." *Journal of Fluid Mechanics*, Vol. 581, 2007, pp. 287-321.

[27]Utturkar, Y., Mittal, R., Rampunggoon, P., and Cattafesta, L., "Sensitivity of Synthetic Jets to the Design of the Jet Cavity." AIAA Paper 2002-0124, 2002.

[28]Mittal, R., Dong, H., Bozkurttas, M., Najjar, F., Vargas, A., and Loebbecke, A., "A Versatile Immersed Boundary Method for Incompressible Flows with Complex Boundaries." *Journal of Computational Physics (under review)*, 2007.

[29]Na, Y., and Moin, P., "Direct Numerical Simulation of a Separated Turbulent Boundary Layer." *Journal of Fluid Mechanics*, Vol. 370, 1998, pp. 175-201.